JCTC Journal of Chemical Theory and Computation

Computational Free Energy Studies of a New Ice Polymorph Which Exhibits Greater Stability than Ice I_h

Christopher J. Fennell and J. Daniel Gezelter*

Department of Chemistry and Biochemistry, University of Notre Dame, Notre Dame, Indiana 46556

Received January 7, 2005

Abstract: The absolute free energies of several ice polymorphs were calculated using thermodynamic integration. These polymorphs are predicted by computer simulations using a variety of common water models to be stable at low pressures. A recently discovered ice polymorph that has as yet *only* been observed in computer simulations (Ice-*i*) was determined to be the stable crystalline state for *all* the water models investigated. Phase diagrams were generated, and phase coexistence lines were determined for all of the known low-pressure ice structures. Additionally, potential truncation was shown to play a role in the resulting shape of the free energy landscape.

1. Introduction

Water has proven to be a challenging substance to depict in simulations, and a variety of models have been developed to describe its behavior under varying simulation conditions.[1−12] These models have been used to investigate important physical phenomena-like phase transitions, transport properties, and the hydrophobic effect.[13−15] With the choice of models available, it is only natural to compare them under interesting thermodynamic conditions in an attempt to clarify the limitations of each.[4,16−18] Two important properties to quantify are the Gibbs and Helmholtz free energies, particularly for the solid forms of water, as these predict the thermodynamic stability of the various phases. Water has a particularly rich phase diagram and takes on a number of different and stable crystalline structures as the temperature and pressure are varied. It is a challenging task to investigate the entire free energy landscape;[19] and ideally, research is focused on the phases having the lowest free energy at a given state point, because these phases will dictate the relevant transition temperatures and pressures for the model.

The high-pressure phases of water (ice II−ice X as well as ice XII) have been studied extensively both experimentally and computationally. In this paper, standard reference state methods were applied in the *low* pressure regime to evaluate the free energies for a few known crystalline water polymorphs that might be stable at these pressures. This work is unique in that one of the crystal lattices was arrived at through crystallization of a computationally efficient water model under constant pressure and temperature conditions. Crystallization events are interesting in and of themselves;[13,20] however, the crystal structure obtained in this case is different from any previously observed ice polymorphs in experiment or simulation.[12] We have named this structure Ice-*i* to indicate its origin in computational simulation. The unit cell of Ice-*i* and an axially elongated variant named Ice-*i*′ both consist of eight water molecules that stack in rows of interlocking water tetramers as illustrated in Figure 1A,B. These tetramers form a crystal structure similar in appearance to a recent two-dimensional surface tessellation simulated on silica.[21] As expected in an ice crystal constructed of water tetramers, the hydrogen bonds are not as linear as those observed in ice I_h; however, the interlocking of these subunits appears to provide significant stabilization to the overall crystal. The arrangement of these tetramers results in octagonal cavities that are typically greater than 6.3 Å in diameter (Figure 2). This open structure leads to crystals that are typically 0.07 g/cm^3 less dense than ice I_h.

Results from our previous study indicated that Ice-*i* is the minimum energy crystal structure for the single point water models investigated (for discussions on these single point dipole models, see our previous work and related articles).[5,8,12] Our earlier results considered only energetic stabilization and neglected entropic contributions to the overall free energy. To address this issue, we have calculated

10.1021/ct050005s CCC: $30.25
Published on Web 04/30/2005

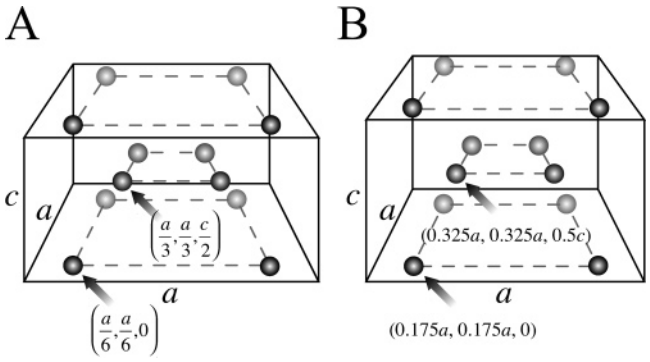

Figure 1. (A) Unit cells for Ice-*i* and (B) Ice-*i*′. The spheres represent the center-of-mass locations of the water molecules. The *a* to *c* ratios for Ice-*i* and Ice-*i*′ are given by 2.1214 and 1.785, respectively.

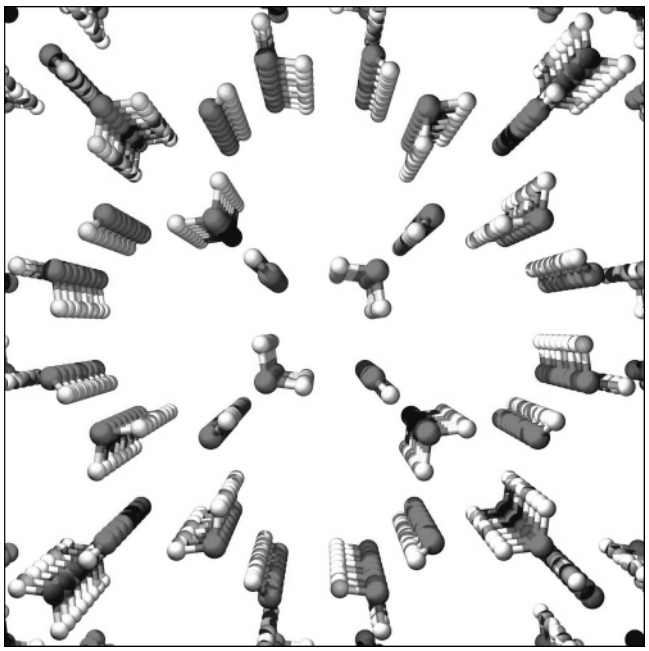

Figure 2. A rendering of a proton ordered crystal of Ice-*i* looking down the (001) crystal face. The presence of large octagonal pores leads to a polymorph that is less dense than ice I_h.

the absolute free energy of this crystal using thermodynamic integration and compared it to the free energies of ice I_c and ice I_h (the common low-density ice polymorphs) and ice B (a higher density but very stable crystal structure observed by Bàez and Clancy in free energy studies of SPC/E).[22] This work includes results for the water model from which Ice-*i* was crystallized (SSD/E) in addition to several common water models (TIP3P, TIP4P, TIP5P, and SPC/E) and a reaction field parametrized single point dipole water model (SSD/RF). The axially elongated variant, Ice-*i*′, was used in calculations involving SPC/E, TIP4P, and TIP5P. The square tetramers in Ice-*i* distort in Ice-*i*′ to form a rhombus with alternating 85 and 95 degree angles. Under SPC/E, TIP4P, and TIP5P, this geometry is better at forming favorable hydrogen bonds. The degree of rhomboid distortion depends on the water model used but is significant enough to split a peak in the radial distribution function which corresponds to diagonal sites in the tetramers.

2. Methods

Canonical ensemble (NVT) molecular dynamics calculations were performed using the OOPSE molecular mechanics program.[23] The densities chosen for the simulations were taken from isobaric−isothermal (NPT) simulations performed at 1 atm and at 200 K. Each model (and each crystal structure) was allowed to relax for 300 ps in the NPT ensemble before averaging the density to obtain the volumes for the NVT simulations. All molecules were treated as rigid bodies, with orientational motion propagated using the symplectic DLM integration method. Details about the implementation of this technique can be found in a recent publication.[24]

Thermodynamic integration was utilized to calculate the Helmholtz free energies (A) of the listed water models at various state points. Thermodynamic integration is an established technique that has been used extensively in the calculation of free energies for condensed phases of materials.[25−29] This method uses a sequence of simulations during which the system of interest is converted into a reference system for which the free energy is known analytically (A_0). The difference in potential energy between the reference system and the system of interest (ΔV) is then integrated in order to determine the free energy difference between the two states:

$$A = A_0 + \int_0^1 \langle \Delta V \rangle_\lambda d\lambda \tag{1}$$

Here, λ is the parameter that governs the transformation between the reference system and the system of interest. For crystalline phases, an harmonically restrained (Einstein) crystal is chosen as the reference state, while for liquid phases, the ideal gas is taken as the reference state.

In an Einstein crystal, the molecules are restrained at their ideal lattice locations and orientations. Using harmonic restraints, as applied by Bàez and Clancy, the total potential for this reference crystal (V_{EC}) is the sum of all the harmonic restraints

$$V_{EC} = \sum_i \left[\frac{K_v}{2}(r_i - r_i^0)^2 + \frac{K_\theta}{2}(\theta_i - \theta_i^0)^2 + \frac{K_\omega}{2}(\omega_i - \omega_i^0)^2 \right] \tag{2}$$

where K_v, K_θ, and K_ω are the spring constants restraining translational motion and deflection of and rotation around the principal axis of the molecule, respectively. These spring constants are typically calculated from the mean-square displacements of water molecules in an unrestrained ice

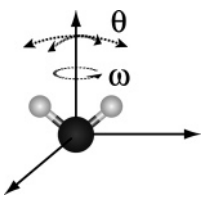

Figure 3. Possible orientational motions for a restrained molecule. θ angles correspond to displacement from the body-frame *z*-axis, while ω angles correspond to rotation about the body-frame *z*-axis. K_θ and K_ω are spring constants for the harmonic springs restraining motion in the θ and ω directions.

Table 1. Calculated Free Energies for Several Ice Polymorphs along with the Calculated Melting (or Sublimation) and Boiling Points for the Investigated Water Models[a]

water model	I_h	I_c	B	Ice-*i*	Ice-*i′*	T_m (*T_s)	T_b
TIP3P	−11.41(2)	−11.23(3)	−11.82(3)	−12.30(3)		269(7)	357(4)
TIP4P	−11.84(3)	−12.04(2)	−12.08(3)		−12.33(3)	262(6)	354(4)
TIP5P	−11.85(3)	−11.86(2)	−11.96(2)		−12.29(2)	266(7)	337(4)
SPC/E	−12.87(2)	−13.05(2)	−13.26(3)		−13.55(2)	299(6)	396(4)
SSD/E	−11.27(2)	−11.19(4)	−12.09(2)	−12.54(2)		*355(4)	
SSD/RF	−11.96(2)	−11.60(2)	−12.53(3)	−12.79(2)		278(7)	382(4)

[a] All free energy calculations used a cutoff radius of 9.0 Å and were performed at 200 K and 1 atm. Units of free energy are kcal/mol, while transition temperature are in Kelvin. Calculated error of the final digits is in parentheses.

crystal at 200 K. For these studies, $K_\nu = 4.29$ kcal mol^{-1} Å^{-2}, $K_\theta = 13.88$ kcal mol^{-1} rad^{-2}, and $K_\omega = 17.75$ kcal mol^{-1} rad^{-2}. It is clear from Figure 3 that the values of θ range from 0 to π, while ω ranges from $-\pi$ to π. The partition function for a molecular crystal restrained in this fashion can be evaluated analytically, and the Helmholtz Free Energy (A) is given by

$$\frac{A}{N} = \frac{E_m}{N} - kT\ln\left(\frac{kT}{h\nu}\right)^3 - kT\ln\left[\pi^{1/2}\left(\frac{8\pi^2 I_A kT}{h^2}\right)^{1/2}\left(\frac{8\pi^2 I_B kT}{h^2}\right)^{1/2}\left(\frac{8\pi I_C kT}{h^2}\right)^{1/2}\right] - kT\ln\left[\frac{kT}{2(\pi K_\omega K_\theta)^{1/2}}\exp\left(-\frac{kT}{2K_\theta}\right)\int_0^{(kT/2K_\theta)^{1/2}}\exp(t^2)\mathrm{d}t\right] \quad (3)$$

where $2\pi\nu = (K_\nu/m)^{1/2}$, and E_m is the minimum potential energy of the ideal crystal.[28] The choice of an Einstein crystal reference state is somewhat arbitrary. Any ideal system for which the partition function is known exactly could be used as a reference point as long as the system does not undergo a phase transition during the integration path between the real and ideal systems. Nada and van der Eerden have shown that the use of different force constants in the Einstein crystal does not affect the total free energy,[30] and Gao et al. have shown that free energies computed with the Debye crystal reference state differ from the Einstein crystal by only a few tenths of a kJ mol^{-1}.[31] These free energy differences can lead to some uncertainty in the computed melting point of the solids.

In the case of molecular liquids, the ideal vapor is chosen as the target reference state. There are several examples of liquid-state free energy calculations of water models present in the literature.[22,26,32,33] These methods typically differ in regard to the path taken for switching off the interaction potential to convert the system to an ideal gas of water molecules. In this study, we applied one of the most convenient methods and integrated over the λ^4 path, where all interaction parameters are scaled equally by this transformation parameter. This method has been shown to be reversible and provide results in excellent agreement with other established methods.[22]

Near the cutoff radius ($0.85*r_{cut}$), charge, dipole, and Lennard-Jones interactions were gradually reduced by a cubic switching function. By applying this function, these interactions are smoothly truncated, thereby avoiding the poor energy conservation which results from harsher truncation schemes. The effect of a long-range correction was also investigated on select model systems in a variety of manners. For the SSD/RF model, a reaction field with a fixed dielectric constant of 80 was applied in all simulations.[34] For a series of the least computationally expensive models (SSD/E, SSD/RF, TIP3P, and SPC/E), simulations were performed with longer cutoffs of 10.5, 12, 13.5, and 15 Å to compare with the 9 Å cutoff results. Finally, the effects of using the Ewald summation were estimated for TIP3P and SPC/E by performing single configuration Particle-Mesh Ewald (PME) calculations[35] for each of the ice polymorphs. The calculated energy difference in the presence and absence of PME was applied to the previous results in order to predict changes to the free energy landscape.

3. Results and Discussion

The calculated free energies of proton-ordered variants of three low-density polymorphs (I_h, I_c, and Ice-*i* or Ice-*i′*) and the stable higher density ice B are listed in Table 1. Ice B was included because it has been shown to be a minimum free energy structure for SPC/E at ambient conditions.[22] In addition to the free energies, the relevant transition temperatures at standard pressure are also displayed in Table 1. These free energy values indicate that Ice-*i* is the most stable state for all of the investigated water models. With the free energy at these state points, the Gibbs−Helmholtz equation was used to project to other state points and to build phase diagrams. Figure 4 is an example diagram built from the results for the TIP3P water model. All other models have similar structure, although the crossing points between the phases move to different temperatures and pressures as indicated from the transition temperatures in Table 1. It is interesting to note that ice I_h (and ice I_c for that matter) do not appear in any of the phase diagrams for any of the models. For purposes of this study, ice B is representative of the dense ice polymorphs. A recent study by Sanz et al. provides details on the phase diagrams for SPC/E and TIP4P at higher pressures than those studied here.[19]

We note that all of the crystals investigated in this study are ideal proton-ordered antiferroelectric structures. All of the structures obey the Bernal-Fowler rules[36] and should be able to form stable proton-*disordered* crystals which have the traditional $k_B\ln(3/2)$ residual entropy at 0 K.[37] Simulations of proton-disordered structures are relatively unstable with all but the most expensive water models.[30] Our simulations have therefore been performed with the ordered antiferroelectric structures which do not require the residual entropy term to be accounted for in the free energies. However, this

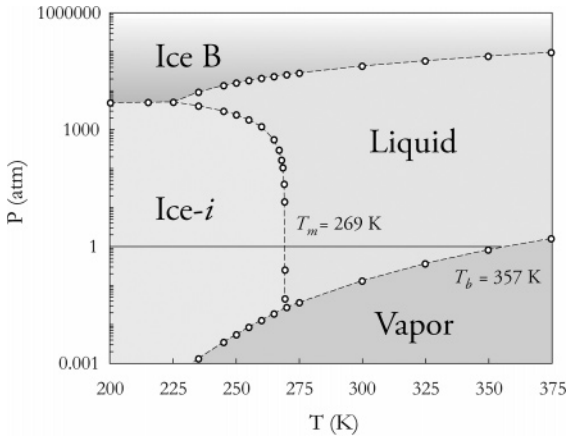

Figure 4. Phase diagram for the TIP3P water model in the low-pressure regime. The displayed T_m and T_b values are good predictions of the experimental values; however, the solid phases shown are not the experimentally observed forms. Both cubic and hexagonal ice *I* are higher in energy and do not appear in the phase diagram.

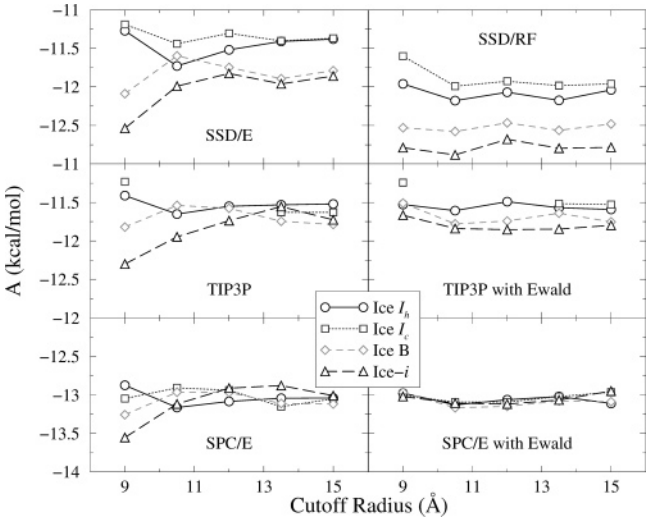

Figure 5. Free energy as a function of cutoff radius for SSD/E, TIP3P, SPC/E, SSD/RF with a reaction field and the TIP3P and SPC/E models with an added Ewald correction term. Error for the larger cutoff points is equivalent to that observed at 9.0 Å (see Table 1). Data for ice I_c with TIP3P using both 12 and 13.5 Å cutoffs were omitted because the crystal was prone to distortion and melting at 200 K. Ice-*i*′ is the form of Ice-*i* used in the SPC/E simulations.

may result in some discrepancies when comparing our melting temperatures to the melting temperatures that have been calculated via thermodynamic integrations of the disordered structures.[19]

Most of the water models have melting points that compare quite favorably with the experimental value of 273 K. The unfortunate aspect of this result is that this phase change occurs between Ice-*i* and the liquid-state rather than ice I_h and the liquid state. These results do not contradict other studies which predict a range of 191 to 238 K for the melting temperature of ice I_h using TIP4P. The range in temperatures can be attributed to choice of interaction truncation and proton ordering.[19,29−31] If the presence of ice B and Ice-*i* were omitted, a T_m value around 200 K would be predicted from this work. However, the T_m from Ice-*i* is calculated to be 262 K, indicating that these simulation based structures ought to be included in studies probing phase transitions with this model. Also of interest in these results is that SSD/E does not exhibit a melting point at 1 atm but does sublime at 355 K. This is due to the significant stability of Ice-*i* over all other polymorphs for this particular model under these conditions. While troubling, this behavior resulted in the spontaneous crystallization of Ice-*i* which led us to investigate this structure. These observations provide a warning that simulations of SSD/E as a "liquid" near 300 K are actually metastable and run the risk of spontaneous crystallization. However, when a longer cutoff radius is used, SSD/E prefers the liquid state under standard temperature and pressure.

For the more computationally efficient water models, we have also investigated the effect of potential trunctaion on the computed free energies as a function of the cutoff radius. As seen in Figure 5, the free energies of the ice polymorphs with water models lacking a long-range correction show significant cutoff dependence. In general, there is a narrowing of the free energy differences while moving to greater cutoff radii. As the free energies for the polymorphs converge, the stability advantage that Ice-*i* exhibits is reduced. Adjacent to each of these plots are results for systems with applied or estimated long-range corrections. SSD/RF was parametrized for use with a reaction field, and the benefit provided by this computationally inexpensive correction is apparent. The free energies are largely independent of the size of the reaction field cavity in this model, so small cutoff radii mimic bulk calculations quite well under SSD/RF.

Although TIP3P was paramaterized for use without the Ewald summation, we have estimated the effect of this method for computing long-range electrostatics for both TIP3P and SPC/E. This was accomplished by calculating the potential energy of identical crystals both with and without particle mesh Ewald (PME). Similar behavior to that observed with reaction field is seen for both of these models. The free energies show reduced dependence on cutoff radius and span a narrower range for the various polymorphs. Like the dipolar water models, TIP3P displays a relatively constant preference for the Ice-*i* polymorph. Crystal preference is much more difficult to determine for SPC/E. Without a long-range correction, each of the polymorphs studied assumes the role of the preferred polymorph under different cutoff radii. The inclusion of the Ewald correction flattens and narrows the gap in free energies such that the polymorphs are isoenergetic within statistical uncertainty. This suggests that other conditions, such as the density in fixed-volume simulations, can influence the polymorph expressed upon crystallization.

4. Conclusions

In this work, thermodynamic integration was used to determine the absolute free energies of several ice polymorphs. The new polymorph, Ice-*i*, was observed to be the stable crystalline state for *all* the water models when using a 9.0 Å cutoff. However, the free energy partially depends on simulation conditions (particularly on the choice of long-

range correction method). Regardless, Ice-*i* was still observed to be either the stable polymorph or one of a set of metastable polymorphs for *all* of the studied water models.

So what is the preferred solid polymorph for simulated water? As indicated above, the answer appears to be dependent both on the conditions and the model used. In the case of short cutoffs without a long-range interaction correction, Ice-*i* and Ice-*i*′ have the lowest free energy of the studied polymorphs with all the models. Ideally, crystallization of each model under constant pressure conditions, as was done with SSD/E, would aid in the identification of their respective preferred structures. This work, however, helps illustrate how studies involving one specific model can lead to insight about important behavior of others.

The stability of Ice-*i* in the SSD models is probably due to wide conical angle over which the short-range sticky potential is attractive. This allows added stability from hydrogen bonding at unrealistic O−H−O angles. The tetramers present in the Ice-*i* structure are *not* in particularly favorable arrangements for the dipolar interactions, so it is unlikely that the dipolar strength of the SSD family is helping to stabilize this structure. Increasing the angular specificity of the attractive portion of the sticky potential by using higher powers of the spherical harmonic term (i.e. $(Y_3^2 + Y_3^{-2})^3$) would be a simple way to destabilize the Ice-*i* structure.

It is possible that one of the newer parametrizations of the point-charge models such as the Nada and van der Eerden six-site model,[30] or the Ewald-corrected versions of the TIP models (e.g. TIP4P-Ew,[38] and TIP5P-E[39]), would also destabilize this structure relative to the correct ice structures. We also note that none of the water models used in this study are polarizable or flexible models. It is entirely possible that the polarizability of real water makes Ice-*i* substantially less stable than ice I_h. However, the calculations presented above seem interesting enough to communicate before the role of polarizability (or flexibility) has been thoroughly investigated.

Finally, due to the stability of Ice-*i* in the investigated simulation conditions, the question arises as to possible experimental observation of this polymorph. The rather extensive past and current experimental investigation of water in the low-pressure regime makes us hesitant to ascribe any relevance to this work outside of the simulation community. It is for this reason that we chose a name for this polymorph which involves an imaginary quantity. That said, there are certain experimental conditions that would provide the most ideal situation for possible observation. These include the negative pressure or stretched solid regime, small clusters in vacuum deposition environments, and in clathrate structures involving small nonpolar molecules. For the purpose of comparison with experimental results, we have calculated the oxygen−oxygen pair correlation function, $g_{OO}(r)$, and the structure factor, $S(\vec{q})$, for the two Ice-*i* variants (along with example ice I_h and I_c plots) at 77 K, and they are shown in Figures 6 and 7 respectively. It is interesting to note that the structure factors for Ice-*i*′ and Ice-I_c are quite similar. The primary differences are small peaks at 1.125, 2.29, and 2.53 Å^{-1}, so particular attention to these regions would be needed to identify the new *i*′ variant from the I_c variant.

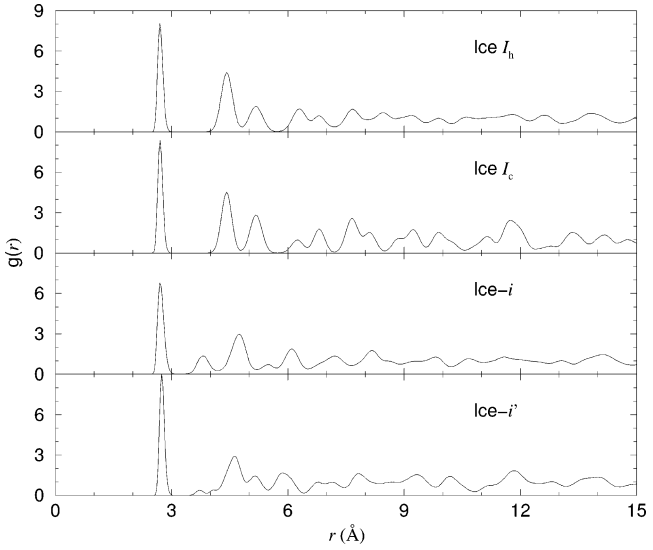

Figure 6. Radial distribution functions of ice I_h, I_c, and Ice-*i* calculated from simulations of the SSD/RF water model at 77 K. The Ice-*i* distribution function was obtained from simulations composed of TIP4P water.

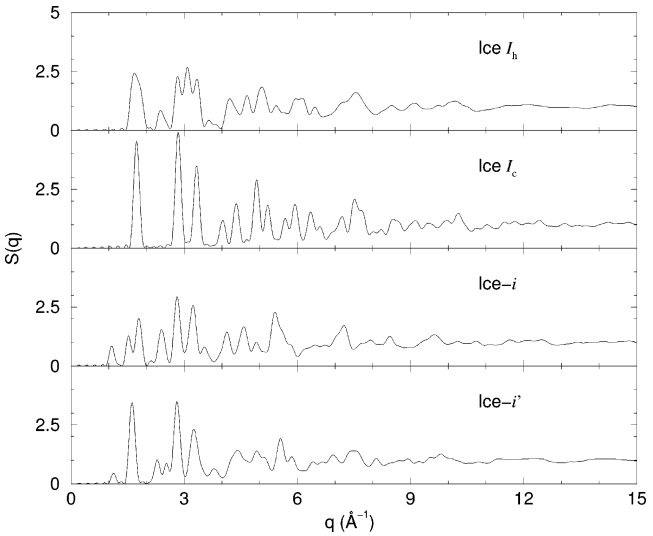

Figure 7. Predicted structure factors for ice I_h, I_c, Ice-*i*, and Ice-*i*′ at 77 K. The raw structure factors have been convoluted with a Gaussian instrument function (0.075 Å^{-1} width) to compensate for the trunction effects in our finite size simulations.

Acknowledgment. Support for this project was provided by the National Science Foundation under grant CHE-0134881. Computation time was provided by the Notre Dame High Performance Computing Cluster and the Notre Dame Bunch-of-Boxes (B.o.B) computer cluster (NSF grant DMR-0079647).

Supporting Information Available: PDB files containing 1024-molecule example structures of proton-ordered Ice-*i* and Ice-*i*′. This material is available free of charge via the Internet at http://pubs.acs.org.

References

(1) Stillinger, F. H.; Rahman, A. *J. Chem. Phys.* **1974**, *60*, 1545−1557.

(2) Rahman, A.; Stillinger, F. H.; Lemberg, H. L. *J. Chem. Phys.* **1975**, *63*, 5223−5230.

(3) Berendsen, H. J. C.; Postma, J. P. M.; van Gunsteren, W. F.; Hermans, J. Simple Point Charge Water. In *Intermolecular Forces*; Pullman, B., Ed.; Reidel: Dordrecht, 1981.

(4) Jorgensen, W. L.; Chandrasekhar, J.; Madura, J. D.; Impey, R. W.; Klein, M. L. *J. Chem. Phys.* **1983**, *79*, 926−935.

(5) Bratko, D.; Blum, L.; Luzar, A. *J. Chem. Phys.* **1985**, *83*, 6367−6370.

(6) Berendsen, H. J. C.; Grigera, J. R.; Straatsma, T. P. *J. Phys. Chem.* **1987**, *91*, 6269−6271.

(7) Caldwell, J. W.; Kollman, P. A. *J. Phys. Chem.* **1995**, *99*, 6208−6219.

(8) Liu, Y.; Ichiye, T. *J. Phys. Chem.* **1996**, *100*, 2723−2730.

(9) van der Spoel, D.; van Maaren, P. J.; Berendsen, H. J. C. *J. Chem. Phys.* **1998**, *108*, 10220−10230.

(10) Urbič, T.; Vlachy, V.; Kalyuzhnyi, Y. V.; Southall, N. T.; Dill, K. A. *J. Chem. Phys.* **2000**, *112*, 2843−2848.

(11) Mahoney, M. W.; Jorgensen, W. L. *J. Chem. Phys.* **2000**, *112*, 8910−8922.

(12) Fennell, C. J.; Gezelter, J. D. *J. Chem. Phys.* **2004**, *120*, 9175−9184.

(13) Yamada, M.; Mossa, S.; Stanley, H. E.; Sciortino, F. *Phys. Rev. Lett.* **2002**, *88*, 195701.

(14) Marrink, S. J.; Berendsen, H. J. C. *J. Phys. Chem.* **1994**, *98*, 4155−4168.

(15) Gallagher, K. R.; Sharp, K. A. *J. Am. Chem. Soc.* **2003**, *125*, 9853.

(16) Jorgensen, W. L.; Jenson, C. *J. Comput. Chem.* **1998**, *19*, 1179−1186.

(17) Báez, L. A.; Clancy, P. *J. Chem. Phys.* **1994**, *101*, 9837−9840.

(18) Mahoney, M. W.; Jorgensen, W. L. *J. Chem. Phys.* **2001**, *114*, 363−366.

(19) Sanz, E.; Vega, C.; Abascal, J. L. F.; MacDowell, L. G. *Phys. Rev. Lett.* **2004**, *92*, 255701.

(20) Matsumoto, M.; Saito, S.; Ohimine, I. *Nature (London)* **2002**, *416*, 409−413.

(21) Yang, J.; Meng, S.; Xu, L. F.; Wang, E. G. *Phys. Rev. Lett.* **2004**, *92*, 146102.

(22) Bàez, L. A.; Clancy, P. *J. Chem. Phys.* **1995**, *103*, 9744−9755.

(23) Meineke, M. A.; II, C. F. V.; Lin, T.; Fennell, C. J.; Gezelter, J. D. *J. Comput. Chem.* **2005**, *26*, 252−271.

(24) Dullweber, A.; Leimkuhler, B.; McLachlan, R. *J. Chem. Phys.* **1997**, *107*, 5840−5851.

(25) Frenkel, D.; Ladd, A. J. C. *J. Chem. Phys.* **1984**, *81*, 3188−3193.

(26) Hermans, J.; Pathiaseril, A.; Anderson, A. *J. Am. Chem. Soc.* **1988**, *110*, 5982−5986.

(27) Meijer, E. J.; Frenkel, D.; LeSar, R. A.; Ladd, A. J. C. *J. Chem. Phys.* **1990**, *92*, 7570−7575.

(28) Bàez, L. A.; Clancy, P. *Mol. Phys.* **1995**, *86*, 385−396.

(29) Vlot, M. J.; Huinink, J.; van der Eerden, J. P. *J. Chem. Phys.* **1999**, *110*, 55−61.

(30) Nada, H.; van der Eerden, J. P. J. M. *J. Chem. Phys.* **2003**, *118*, 7401−7413.

(31) Gao, G. T.; Zeng, X. C.; Tanaka, H. *J. Chem. Phys.* **2000**, *112*, 8534−8538.

(32) Quintana, J.; Haymet, A. D. J. *Chem. Phys. Lett.* **1992**, *189*, 273−277.

(33) Mezei, M. *J. Comput. Chem.* **1992**, *13*, 651.

(34) Onsager, L. *J. Am. Chem. Soc.* **1936**, *58*, 1486-1493.

(35) Ponder, J. W.; Richards, F. M. *J. Comput. Chem.* **1987**, *8*, 1016−1024.

(36) Bernal, J. D.; Fowler, R. H. *J. Chem. Phys.* **1933**, *1*, 515−548.

(37) Pauling, L. *J. Am. Chem. Soc.* **1935**, *57*, 2680−2684.

(38) Horn, H. W.; Swope, W. C.; Pitera, J. W.; Madura, J. D.; Dick, T. J.; Hura, G. L.; Head-Gordon, T. *J. Chem. Phys.* **2004**, *120*, 9665−9678.

(39) Rick, S. W. *J. Chem. Phys.* **2004**, *120*, 6085−6093.

CT050005S